Efficient and Stable Optimization of Multi-pass End Milling Using a Cloud Drop-Enabled Particle Swarm Optimization Algorithm

CAI Xulin, YANG Wenan, HUANG Chao*

National Key Laboratory of Science and Technology on Helicopter Transmission, Nanjing University of Aeronautics and Astronautics, Nanjing 210016, P.R. China

(Received 19 May 2020; revised 22 December 2020; accepted 15 January 2021)

Abstract: Optimization of machining parameters is of great importance for multi-pass end milling because machining parameters adversely or positively affect the time and quality of production. This paper develops a second-order full-discretization method (2ndFDM)-based 3-D stability prediction model for simultaneous optimization of spindle speed, axial cutting depth and radial cutting depth. The optimal machining parameters in each pass are obtained to achieve the minimum production time comprehensive considering constraints of 3-D stability, machine tool performance, tool life and machining requirements. A cloud drop-enabled particle swarm optimization (CDPSO) algorithm is proposed to solve the developed machining parameter optimization, and 13 benchmark problems are used to evaluate CDPSO algorithm. Numerical results show that CDPSO algorithm has a certain advantage in computational cost as well as comparable search quality and robustness. A demonstrative example is provided.

Key words: machining parameter; multi-pass end milling; chatter stability; particle swarm optimization (PSO); cloud model

CLC number: TG5 **Document code:** A **Article ID:** 1005-1120(2021)03-0462-12

0 Introduction

Optimization of machining parameters that adversely or positively affect the machining process behavior is of great importance to shorten the production time, explore the production potential and improve the efficiency of multi-pass end milling operation. Over the past few decades, a number of researchers have contributed significant research in the formulation of machining parameter optimization models and in the design of their solution algorithms, claiming to have made headway in their respective machining operations[1-3]. However, most current researches are focused on how to solve the parameter optimization model efficiently, while little attention is paid to improve the practicality of optimization model. Taking milling operations for example, most of the related literatures simplified the milling operation to symmetrical milling, and most optimization models did not consider the constraint of machining stability. For large, complex, thin-walled structures, such as helicopter rotor blades and aircraft envelope, however, chatter easily occurs and results in poor surface quality and machining inaccuracy because of low rigidity of this kind of structure.

How to avoid chatter occurrence in the machining process is a challenging issue and has caught the attention of researchers and technicians in the field of machining. The most common method is to predict the machining stability lobe diagrams (SLD), and many methods have been proposed[4-5]. Unfortunately, all of these researches are devoted to machining parameter selection in the stability domain without considering production time and quality. Bu-

*Corresponding author, E-mail address: dreamflow@nuaa.edu.cn.

How to cite this article: CAI Xulin, YANG Wenan, HUANG Chao. Efficient and stable optimization of multi-pass end milling using a cloud drop-enabled particle swarm optimization algorithm[J]. Transactions of Nanjing University of Aeronautics and Astronautics, 2021, 38(3): 462-473.

http://dx.doi.org/10.16356/j.1005-1120.2021.03.010

dak et al.[6] and Chen et al.[7] built mathematical model of optimization on machining parameters with the constraint of machining stability to seek the optimal combination of axial cutting depth and radial cutting depth without chatter for the maximum material removal rate, but only two variables were considered in these studies. The three variables related to machining stability, i.e., axial cutting depth, radial cutting depth, and spindle speed are equally important, as they all directly affect the rationality of the parameters obtained. Thus, an accurate three-dimensional (3-D) stability model is established in this paper for the optimization of multi-pass end machining parameters.

In recent years, particle swarm optimization (PSO) and its variants have been successfully developed to tackle different optimization problems[8-9]. Although PSO appears to be fast in finding solutions near optimal, it is weak in subsequent exploitation. This study proposed a cloud drop-enabled PSO (CDPSO) algorithm inspired by the excellent properties of the normal cloud model[10], which can effectively improve the randomness and fuzziness of the particle evolution. Numerical results obtained using the proposed CDPSO algorithm to solve benchmark problems indicate that it performs better than other four existing algorithms. And a demonstrative example shows that optimal parameters obtained by the proposed optimization model performs better than empirical parameters by 34% with respect to production time.

1 3-D Milling Stability Model

Considering that the degree of freedom most concerned in machining is only the one perpendicular to the machined surface. Therefore, the milling dynamic model used in this study is based on the dynamic equation described as follows

$$\ddot{\boldsymbol{x}}(t)+2\zeta w_{\mathrm{n}}\dot{\boldsymbol{x}}(t)+w_{\mathrm{n}}^{2}\boldsymbol{x}(t)=-\frac{dh(t)}{m_{\mathrm{t}}}(\boldsymbol{x}(t)-\boldsymbol{x}(t-T)) \tag{1}$$

where ζ is the relative damping; w_{n} the angular natural frequency; d the axial cutting depth; m_{t} the modal mass of the tool; T the regenerative delay and $h(t)$ a specific cutting force coefficient expressed as

$$h(t)=\sum_{j=1}^{Z}g(\varphi_j(t))\sin(\varphi_j(t))\cdot[K_{\mathrm{t}}\cos(\varphi_j(t))+K_{\mathrm{n}}\cos(\varphi_j(t))] \tag{2}$$

here Z is the number of the cutter teeth; K_{t} and K_{n} are the tangential and normal cutting force coefficients, respectively; $g(\varphi_j(t))$ is a window function involving the angular position of the jth tooth

$$g(\varphi_j(t))=\begin{cases}1 & \varphi_{\mathrm{st}}<\varphi_j(t)<\varphi_{\mathrm{ex}}\\ 0 & \text{Otherwise}\end{cases} \tag{3}$$

where φ_{st} and φ_{ex} are the start and exit angles, respectively; for up-milling, $\varphi_{\mathrm{st}}=0$ and $\varphi_{\mathrm{ex}}=\arccos(1-2a/D)$; for down-milling, $\varphi_{\mathrm{st}}=\arccos(2a/D-1)$ and $\varphi_{\mathrm{ex}}=\pi$, where a/D is the radial immersion ratio.

Without loss of generality, Eq.(1) can be expressed as state-space form

$$\dot{\boldsymbol{x}}(t)=\boldsymbol{A}_{\mathrm{n}}\boldsymbol{x}(t)+\boldsymbol{A}(t)\boldsymbol{x}(t)-\boldsymbol{A}(t)\boldsymbol{x}(t-T) \tag{4}$$

where

$$\begin{cases}\boldsymbol{A}_{\mathrm{n}}=\begin{bmatrix}-\zeta w_{\mathrm{n}} & 1/m_{\mathrm{t}}\\ m_{\mathrm{t}}(\zeta w_{\mathrm{n}})^{2}-m_{\mathrm{t}}w_{\mathrm{n}}^{2} & -\zeta w_{\mathrm{n}}^{2}\end{bmatrix}\\ \boldsymbol{A}(t)=\begin{bmatrix}0 & 0\\ -wh(t) & 0\end{bmatrix}\\ \boldsymbol{x}(t)=\begin{bmatrix}x(t)\\ m_{\mathrm{t}}(\dot{x}(t)+\zeta w_{\mathrm{n}}x(t))\end{bmatrix}\end{cases} \tag{5}$$

The response of Eq.(4) on $t\in[k\tau,(k+1)\tau]$ can be expressed as

$$\boldsymbol{x}(t)=\mathrm{e}^{\boldsymbol{A}_{\mathrm{n}}(t-k\tau)}\boldsymbol{x}(k\tau)+\int_{k\tau}^{t}\{\mathrm{e}^{\boldsymbol{A}_{\mathrm{n}}(t-\zeta)}\boldsymbol{A}(\zeta)\cdot[\boldsymbol{x}(\zeta)-\boldsymbol{x}(\zeta-T)]\}\mathrm{d}\zeta \tag{6}$$

In a similar way

$$\boldsymbol{x}(k\tau+\tau)=\mathrm{e}^{\boldsymbol{A}_{\mathrm{n}}\tau}\boldsymbol{x}(k\tau)+\int_{0}^{\tau}\{\mathrm{e}^{\boldsymbol{A}_{\mathrm{n}}\zeta}\boldsymbol{A}(k\tau+\tau-\zeta)\cdot[\boldsymbol{x}(k\tau+\tau-\zeta)-\boldsymbol{x}\cdot(k\tau+\tau-\zeta-T)]\}\mathrm{d}\zeta \tag{7}$$

where $t\in[0,\tau]$. The following equations can be obtained by handling the Duhamel term of Eq.(7) with the method described by using second-order full-discretization method (2ndFDM)[4].

$$\boldsymbol{A}(k\tau+\tau-\zeta)=\boldsymbol{A}_{0}^{(k)}+\boldsymbol{A}_{1}^{(k)}\zeta\boldsymbol{x}(k\tau+\tau-\zeta-T)=\boldsymbol{x}_{k+1-m}+\zeta(\boldsymbol{x}_{k-m}-\boldsymbol{x}_{k+1-m})/\tau\,\boldsymbol{x}(k\tau+\tau-\zeta)=\zeta(\zeta-\tau)\boldsymbol{x}_{k-1}/2\tau^{2}+\zeta(2\tau-\zeta)\boldsymbol{x}_{k}/\tau^{2}+(\tau-\zeta)(2\tau-\zeta)\boldsymbol{x}_{k+1}/2\tau^{2} \tag{8}$$

where $\boldsymbol{A}_{0}^{(k)}=\boldsymbol{A}_{k+1}$, $\boldsymbol{A}_{1}^{(k)}=(\boldsymbol{A}_{k}-\boldsymbol{A}_{k+1})/\tau$; $\boldsymbol{A}_{k}$ de-

notes the value of $\boldsymbol{A}(t)$ sampled at $t_k=k\tau$; $\boldsymbol{x}_{k-m}$ and $\boldsymbol{x}_{k+1-m}$ mean the values at $(k-m)\tau$ and $(k+1-m)\tau$, respectively; $\boldsymbol{x}_{k-1}$, $\boldsymbol{x}_k$ and $\boldsymbol{x}_{k+1}$ denote the state item at $(k-1)\tau$, $k\tau$ and $(k+1)\tau$, respectively.

Substituting Eq.(8) into Eq.(7) leads to

$$\boldsymbol{x}_{k+1}=F_{k+1}\boldsymbol{x}_{k+1}+(F_0+F_{0,k})\boldsymbol{x}_k+F_{k-1}\boldsymbol{x}_{k-1}-F_{k+1-m}\boldsymbol{x}_{k+1-m}-F_{k-m}\boldsymbol{x}_{k-m} \quad (9)$$

where

$$F_{k+1}=\left(\boldsymbol{\Phi}_0-\frac{3\boldsymbol{\Phi}_1}{2\tau}+\frac{\boldsymbol{\Phi}_2}{2\tau^2}\right)\boldsymbol{A}_0^{(k)}+\left(\boldsymbol{\Phi}_1-\frac{3\boldsymbol{\Phi}_2}{2\tau}+\frac{\boldsymbol{A}_n^{-1}\left(\tau^3\boldsymbol{\Phi}_3-3\boldsymbol{\Phi}_2\right)}{2\tau^2}\right)\boldsymbol{A}_1^{(k)}$$

$$F_0=\boldsymbol{\Phi}_4$$

$$F_{0,k}=\left(\frac{2\boldsymbol{\Phi}_1}{\tau}-\frac{\boldsymbol{\Phi}_2}{\tau^2}\right)\boldsymbol{A}_0^{(k)}+\left(\frac{2\boldsymbol{\Phi}_2}{\tau}-\frac{\boldsymbol{A}_n^{-1}\left(\tau^3\boldsymbol{\Phi}_3-3\boldsymbol{\Phi}_2\right)}{\tau^2}\right)\boldsymbol{A}_1^{(k)}$$

$$F_{k-1}=\left(\frac{\boldsymbol{\Phi}_2}{2\tau^2}-\frac{\boldsymbol{\Phi}_1}{2\tau}\right)\boldsymbol{A}_0^{(k)}+\left(\frac{\boldsymbol{A}_n^{-1}\left(\tau^3\boldsymbol{\Phi}_3-3\boldsymbol{\Phi}_2\right)}{2\tau^2}-\frac{\boldsymbol{\Phi}_2}{2\tau}\right)\boldsymbol{A}_1^{(k)}$$

$$F_{k+1-m}=\left(\boldsymbol{\Phi}_0-\frac{\boldsymbol{\Phi}_1}{\tau}\right)\boldsymbol{A}_0^{(k)}+\left(\boldsymbol{\Phi}_1-\frac{\boldsymbol{\Phi}_2}{\tau}\right)\boldsymbol{A}_1^{(k)}$$

$$F_{k-m}=\frac{\boldsymbol{\Phi}_1}{\tau}\boldsymbol{A}_0^{(k)}+\frac{\boldsymbol{\Phi}_2}{\tau}\boldsymbol{A}_1^{(k)}$$

where

$$\boldsymbol{\Phi}_0=\boldsymbol{A}_n^{-1}(e^{\boldsymbol{A}_n\tau}-1) \qquad \boldsymbol{\Phi}_1=\boldsymbol{A}_n^{-1}(\tau e^{\boldsymbol{A}_n\tau}-\boldsymbol{\Phi}_0)$$

$$\boldsymbol{\Phi}_2=\boldsymbol{A}_n^{-1}(\tau^2 e^{\boldsymbol{A}_n\tau}-2\boldsymbol{\Phi}_1) \qquad \boldsymbol{\Phi}_3=e^{\boldsymbol{A}_n\tau}$$

Thereafter, the discrete map can be described as

$$\boldsymbol{X}_{k+1}=\boldsymbol{D}_k\boldsymbol{X}_k \quad (10)$$

where

$$\boldsymbol{X}_k=\mathrm{col}(\boldsymbol{x}_k,\boldsymbol{x}_{k-1},\cdots,\boldsymbol{x}_{k+1-m},\boldsymbol{x}_{k-m}) \quad (11)$$

$$\boldsymbol{D}_k=\begin{bmatrix}\boldsymbol{\delta}(F_0+F_{0,k}) & \boldsymbol{\delta}F_{k-1} & 0 & \cdots & 0 & -\boldsymbol{\delta}F_{k+1-m} & -\boldsymbol{\delta}F_{k-m}\\ I & 0 & 0 & \cdots & 0 & 0 & 0\\ 0 & I & 0 & \cdots & 0 & 0 & 0\\ \vdots & \vdots & \vdots & \ddots & \vdots & \vdots & \vdots\\ 0 & 0 & 0 & \cdots & 0 & 0 & 0\\ 0 & 0 & 0 & \cdots & I & 0 & 0\\ 0 & 0 & 0 & \cdots & 0 & I & 0\end{bmatrix} \quad (12)$$

where $\boldsymbol{\delta}=[\boldsymbol{I}-F_{k+1}]^{-1}$ and the transition matrix within a periodic time interval can be established by using the sequence of discrete maps $\boldsymbol{D}_k(k=0,1,2,\cdots,m-1)$, which can be utilized to predict the chatter stability region about spindle speed and axial cutting depth via Floquet theory.

The third variable of the 3-D stability model is the radial immersion ratio a/D, where $a\in(0,D]$. In order to obtain the ideal stability model, an infinitesimal quantity sm is defined for facilitating modeling. The value range is equally divided into ε small pieces, thus

$$\boldsymbol{a}=\mathrm{row}(sm,sm+(D-sm)/\varepsilon,\cdots,D-(D-sm)/\varepsilon,D) \quad (13)$$

At this point, the formulation of 2ndFDM-based 3-D stability model of spindle speed, axial cutting depth and radial cutting depth has been completed.

2 Optimization Model

2.1 Objective functions

In the case of milling, the production time has always been considered as the objective functions in most attempts to optimize the machining parameters. And first of all, it is necessary to construct the model about the length of tool travel.

The length of tool travel in rough pass can be expressed as

$$L_r=\mathrm{GInt}\left(\frac{W}{a_r}\right)L+\mathrm{SInt}\left(\frac{W}{a_r}\right)a_r+a_p+e \quad (14)$$

where a_r is the radial cutting depth in rough machining; a_p the approach distance; and e an arbitrary set distance to avoid possible accidents and damage, which is taken as 2 mm in this study; $\mathrm{GInt}(\cdot)$ and $\mathrm{SInt}(\cdot)$ denote the greatest and the smallest integer operators, respectively.

The approach distance can be expressed as

$$a_p = \sqrt{\left(\frac{D}{2}\right)^2 - \left(\frac{D}{2} - a_r\right)^2} \tag{15}$$

where D is the diameter of the tool.

The travel length of the finish pass is measured from the contact of tool and workpiece to separation

$$L_s = \mathrm{GInt}\left(\frac{W}{a_s}\right)L + \mathrm{SInt}\left(\frac{W}{a_s}\right)a_s + D + e \tag{16}$$

where a_s is the radial cutting depth in finish pass.

The production time can be expressed as

$$T_{total} = T_p + T_L + T_a + T_m + T_r \tag{17}$$

where T_p (minute) is the preparation time, T_L the clamping time, T_a the adjustment time, T_m the machining time, and T_r the tool changing time. Since T_p and T_L are always fixed and have no effect on the total production time, they can be ignored.

Considering that machining operation of multi-pass end milling consists n rough passes and one finish pass, it can be obtained that

$$\begin{cases} T_a = \sum_{i=1}^{n} t_{ari} + t_{as} \\ T_m = \sum_{i=1}^{n} t_{mri} + t_{ms} \\ T_r = \sum_{i=1}^{n} t_{rri} + t_{rs} \end{cases} \tag{18}$$

Substituting Eq.(18) into Eq.(17), the objective function can be expressed as

$$T_{total} = \sum_{i=1}^{n} (t_{ari} + t_{mri} + t_{rri}) + (t_{as} + t_{ms} + t_{rs}) \tag{19}$$

where

$$\begin{cases} t_{ari} = h_1 L_{ri} + h_2, t_{as} = h_1 L_s + h_2 \\ t_{mri} = \dfrac{L_{ri}}{\Omega_{ri} f_{tri} Z}, t_{ms} = \dfrac{L_s}{\Omega_s f_{ts} Z} \\ t_{rri} = Z T_{tc} \dfrac{t_{mri}}{t_{ri}}, t_{rs} = Z T_{tc} \dfrac{t_{ms}}{t_s} \end{cases} \tag{20}$$

where h_1 (minutes per millimeter) and h_2 (minutes) are constants related to tool travel and approach/depart time, which are taken as 7E—4 and 0.3 in this study; Ω_s is the spindle speed (revolution per minute), f_{ts} the feed rate per tooth (millimeters per tooth), Z the number of cutter teeth; and T_{tc} the tool changing time (minutes per tooth) required for each edge and taken as 1.5 in this study; t_{ri} and t_s are the tool life[11] in rough and finish pass, respectively, which can be calculated by

$$\begin{cases} t_{ri} = \left(\dfrac{1\,000 C_v K_v D^{q_v - 1}}{\pi \Omega_{ri} d_{ri}^{x_v} f_{tri}^{y_v} a_{ri}^{s_v} Z^{p_v}}\right)^{\frac{1}{l}} \\ t_s = \left(\dfrac{1\,000 C_v K_v D^{q_v - 1}}{\pi \Omega_s d_s^{x_v} f_{ts}^{y_v} a_s^{s_v} Z^{p_v}}\right)^{\frac{1}{l}} \end{cases} \tag{21}$$

where $C_v, K_v, x_v, y_v, s_v, q_v, p_v$ and l are constants and exponents associated with the tool and workpiece material.

2.2 Constraint functions

To ensure the safety of machining process and the quality of product, including spindle speed, feed rate, axial cutting depth, radial cutting depth, machining force, machining torque, machining power, surface roughness and tool life must be selected within a predetermined interval. The description of the above constraints can be found[11], and it will not be repeated in this paper. In addition to the above constraints, the optimization model constructed in this study also contains three-dimensional machining stability region constraint on spindle speed, axial cutting depth and radial cutting depth, which is described in the previous section.

2.3 Optimization model

Objective function

$$T_{total} = \mathrm{Minimum} \tag{22}$$

Constraint functions

$$\begin{cases} F_{ri} - F_{max} \leqslant 0 \\ F_s - F_{max} \leqslant 0 \\ T_{mri} - T_{mmax} \leqslant 0 \\ T_{ms} - T_{mmax} \leqslant 0 \\ p_{ri} - p_{max} \leqslant 0 \\ p_s - p_{max} \leqslant 0 \\ R_{ri} - R_{rmax} \leqslant 0 \\ R_s - R_{smax} \leqslant 0 \\ T_r - t_{ri} \leqslant 0 \\ T_r - t_s \leqslant 0 \\ d_t = \sum_{i=1}^{n} d_{ri} + d_s \end{cases} \tag{23}$$

where F_{ri}, F_s and F_{max} are the machining forces of the ith rough pass, finish pass and available maximum value, respectively; T_{mri}, T_{ms} and T_{mmax} are the machining torques of the ith rough pass, finish pass, and available maximum value, respectively; p_{ri}, p_s

and p_{max} the machining powers of the ith rough pass, finish pass, and available maximum value, respectively; R_{ri}, R_s, R_{rmax} and R_{smax} the surface roughnesses of the ith rough pass, finish pass, required value in rough pass and finish pass, respectively; t_{ri}, t_s and T_r the tool lifes of the ith rough pass, finish pass and required value, respectively; and d_t d_{ri} and d_s the total axial cutting depth, axial cutting depths of the ith rough pass and finish pass, respectively.

Decision variables: n, d_{ri}, a_{ri}, Ω_{ri}, f_{ri}, d_s, a_s, Ω_s, f_s, where n is the number of rough passes; a_{ri} and a_s are the radial cutting depths of the ith rough pass and finish pass, respectively, Ω_{ri} and Ω_s the spindle speeds of the ith rough pass and finish pass, respectively, and f_{ri} and f_s the feed rates of the ith rough pass and finish pass, respectively.

Before searching for optimal values of decision parameters and minimization production time, the first issue is to obtain the optimal number of passes and the optimal distribution of total stock. Thus, a methodology is implemented to accomplish this task.

If the difference between total axial cutting depth and axial cutting depth of finish pass is divisible by axial cutting depth of rough pass, n equals the corresponding integer quotient; Otherwise, rounds the quotient to the nearest integer in the direction of positive infinity as n, and the axial cutting depth of the last rough machining is equal to the total cutting depth minus the depth of the finishing and the depth of the first $(n-1)$ rough passes.

3 Solution Method and Its Performance Evaluation

3.1 Solution method

Fig.1 is an overall flowchart of the proposed CDPSO algorithm for parameter optimization. First, initialize personal best solution (pbest) of each particle and global best solution (gbest) of the whole swarm. Second, perform cloud mutation operator and two-point crossover operator on particles to generate new particles, and update swarm based on PSO and niching-gene-algorithm-based tournament selection (NGATS)[12] strategy. Finally,

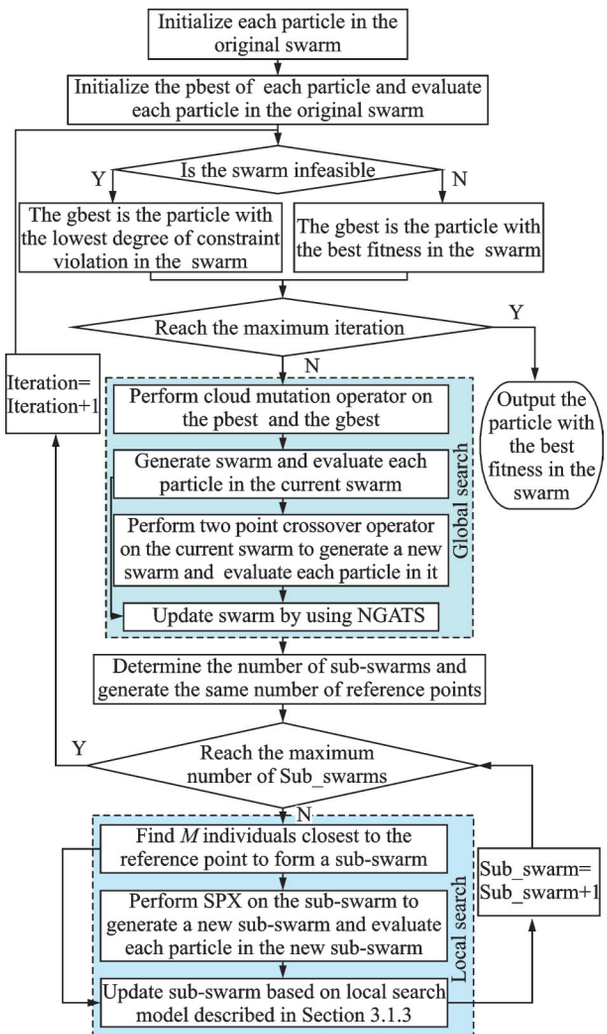

Fig.1 Framework of the proposed CDPSO algorithm

perform simplex crossover (SPX)[13] operator on particles to generate new particles, and update swarm based on dominant particle replacement mechanism.

The proposed CDPSO algorithm is based on an improved version of PSO, which can be described as

$$\begin{cases} \boldsymbol{v}_i^{k+1} = w\boldsymbol{v}_i^k + c_1 \cdot \text{rand}() \cdot (\boldsymbol{p}_i^k - \boldsymbol{x}_i^k) + c_2 \cdot \text{rand}() \cdot \\ \qquad (\boldsymbol{p}_g^k - \boldsymbol{x}_i^k) \\ \boldsymbol{x}_i^{k+1} = \boldsymbol{x}_i^k + \boldsymbol{v}_i^{k+1} \\ w = w_{max} - \dfrac{w_{max} - w_{min}}{\text{IterNumMax}^2} \cdot \text{IterNum}^2 \end{cases} \tag{24}$$

where $\boldsymbol{p}_g^k$ is the gbest of the whole swarm in the kth iteration, $\boldsymbol{p}_i^k$ the pbest of the ith particle in the kth iteration, and rand() the random numbers uniformly distributed between 0 and 1. w denotes inertia weight factor, and decreases gradually with the increase of the square of iteration numbers. IterNum

is the current number of iteration and IterNumMax the maximum number of iterations. In this study, $w_{\max}=0.9, w_{\min}=0.4$.

3.1.1 Constraints handing

Since the optimization of machining parameters involves lots of constraints while PSO is not a constrained optimization algorithm, a simple and efficient constraint processing scheme is implemented in this study, that is, converting multi-constraint and single-objective optimization problem into bi-objective optimization problem to minimize the initial objective $f(\boldsymbol{p}_i)$ and the degree of constraint violation $G(\boldsymbol{p}_i)$ simultaneously. For the sake of clarity, let $\boldsymbol{f}(\boldsymbol{p}_i)=(f(\boldsymbol{p}_i), G(\boldsymbol{p}_i))$. If there only exist inequality constraints, $G(\boldsymbol{p}_i)$ can be expressed as

$$\begin{cases} G(\boldsymbol{p}_i)=\sum_{j=1}^{c} G_j(\boldsymbol{p}_i) \\ G_j(\boldsymbol{p}_i)=\max\{0, g_j(\boldsymbol{p}_i)\} \end{cases} \tag{25}$$

where c is the total number of constraints in a specified problem and $g_j(\boldsymbol{p}_i)$ the jth constraint. Hence, $\boldsymbol{p}_i^*$ is considered as the global optimal (minimum) solution if and only if $G(\boldsymbol{p}_i^*)=0$ and $\neg G(\boldsymbol{p}_i)=0$ such that $f(\boldsymbol{p}_i)\leqslant f(\boldsymbol{p}_i^*)$. Additionally, if there exist equality constraints, convert them into inequality constraints as $|h(\boldsymbol{x})|-\delta\leqslant 0$, where $\delta=1.0\mathrm{E}-4$.

3.1.2 Genetic manipulation

The two-point crossover operator and SPX operator are utilized to process particles in global search and local search, respectively, to increase the diversity of swarm. Besides, a cloud mutation operation is proposed to process the pbest $\boldsymbol{p}_i^k$ and the gbest $\boldsymbol{p}_g^k$ in this study, because it can unify the fuzziness and randomness, and can transform between qualitative concepts and quantitative data, thus, the cloud mutation operation can efficiently improve the uncertainty of evolution. The detail is expressed as

$$\mathrm{En}=\mathrm{En}_{max}-\frac{\mathrm{En}_{max}-\mathrm{En}_{\min}}{\mathrm{IterNumMax}}\times\mathrm{IterNum} \tag{26}$$

$$\mathrm{He}=\mathrm{He}_{max}-\frac{\mathrm{He}_{max}-\mathrm{He}_{\min}}{\mathrm{IterNumMax}}\times\mathrm{IterNum} \tag{27}$$

$$\mathrm{En}'=N(\mathrm{En}, \mathrm{He}^2) \tag{28}$$

$$\boldsymbol{p}_g^k=N(\boldsymbol{p}_g^k, \mathrm{En}'^2) \tag{29}$$

$$\boldsymbol{p}_{ci,l}^k=N(\boldsymbol{p}_{i,l}^k, \mathrm{En}'^2) \tag{30}$$

$$\boldsymbol{p}_{i,l}^k=\begin{cases} \boldsymbol{p}_{ci,l}^k & \mathrm{rand}()<1/n \\ \boldsymbol{p}_{i,l}^k & \mathrm{rand}()\geqslant 1/n \end{cases} \tag{31}$$

$\boldsymbol{p}_g^k$ and $\boldsymbol{p}_{i,l}^k$ (the lth gene locus of $\boldsymbol{p}_i^k$) are reined by cloud drop generated by normal cloud model described in Eqs.(28—30). En and He indicate entropy and hyper entropy, respectively. They decrease with the increase of iteration number as described in Eqs. (26—27), leading to the decrease of En′. Thus, the explorative ability is maintained at a high level in the early stage and kept a global convergence in the later. The operation object of mutation on $\boldsymbol{p}_g^k$ is the whole chromosome and that on $\boldsymbol{p}_i^k$ is the part of gene locus, as shown in Eqs.(29—31). Taking the lth gene locus as an example, the probability of mutation is $1/n$, where n is the total number of design variables. In this study, $\mathrm{En}_{\max}=5.0\mathrm{E}-3$, $\mathrm{En}_{\min}=5.0\mathrm{E}-7$, $\mathrm{He}_{\max}=3.0\mathrm{E}-3$, $\mathrm{He}_{\min}=3.0\mathrm{E}-7$, and the number of generated cloud drop in each iteration is 200.

3.1.3 Evolutionary strategy

In addition to the particle swarm evolution strategy, we use NGATS as a global updating strategy to maintain the balance between selection pressure and diversity of the swarm. However, when solving the problem of low proportion of feasible solutions, such as machining parameter optimization, NGATS always leads to the problem of slow convergence. To handle this situation, a local search model based on clustering partition mechanism is introduced into the current algorithm. The schematic diagram of this mechanism is shown in Fig.2.

Under this mechanism, the swarm of size is divided into n disjoint sub-swarms based on their loca-

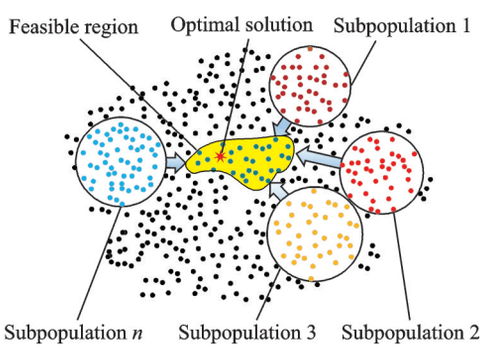

Fig.2 Schematic diagram of the local search model

tions. Then, particles in each sub-swarm of size M are used to generate the same number of offspring of size M' through genetic manipulation. Appropriate evolutionary mechanisms are also introduced to guide the direction of evolution. Besides, only dominant particles are taken account in this strategy for they represent the most important characteristics of the swarm. Hence, after dominant particles are selected from the swarm, they are used to replace particles dominated. The illustration of the updating strategy is as follows.

(1) Initialize the size of sub-swarm M.

(2) Randomly generate N/M reference points for the construction of sub-swarm.

(3) While the maximum number of sub-swarms has not been reached:

Do

① Find M particles closest to the reference point to form a sub-swarm.

② Generate offspring through SPX.

③ Select dominant particles $\overline{x}_i(i=1,\cdots,m)$ from offspring swarm.

(a) Let selected offspring replace the particles in parent particles dominated by them.

(b) Put the evolved sub-swarm in the new swarm.

(c) If the maximum number of sub-swarms reaches, go to the next step; else number of sub-swarms plus one, operate Step 2 again.

(4) End while

(5) Output the local searched swarm.

3.2 Performance evaluation

3.2.1 Benchmark problems

To examine the performance of the proposed CDPSO algorithm, it is tested on 13 most commonly used benchmark problems algorithm[14]. The test results of the proposed CDPSO algorithm are compared with four existing well-known algorithms to evaluate its performance. Before evaluation, the following parameters are selected after a few numbers of trial: Acceleration coefficients $c_1=1.0$ and $c_2=0.5$, the maximum and the minimum inertia weight $w_{\max}=0.9$ and $w_{\min}=0.4$, the probability of the crossover operation in the global search model is 0.8, the probability of mutation operation for the gbest and pbest is 1.0 and 0.2, respectively. In addition, the probability of crossover operation in the local search model is 1.0. The maximum number of iterations, IterNumMax, sizes of swarm N and sub-swarm q are listed in Table 1, which depends on the different characteristics of 13 benchmark problems, respectively. And then fitness function evaluations (FFEs) of these benchmark problems can be obtained. Besides, FFEs of the algorithms in the literatures are also listed in Table 1 to evaluate the computational cost of CDPSO algorithm.

Table 1 IterNumMax, N, q and FFEs of CDPSO and other algorithms

Function	CDPSO				FFE			
	N	q	IterNumMax	FFE	SACABC[15]	M-ABC[16]	COMDE[17]	LCA[18]
g01	65	13	1 500	97 500			130 000	
g02	240	15	1 500	360 000			200 000	
g03	90	9	1 000	90 000			150 000	
g04	50	5	900	45 000			50 000	
g05	96	12	1 850	177 600			200 000	
g06	160	10	600	96 000			12 000	
g07	100	10	1 800	180 000	240 000	240 000	200 000	225 000
g08	25	5	140	3 500			4 000	
g09	50	10	1 200	60 000			70 000	
g10	200	10	2 000	240 000			200 000	
g11	40	12	600	24 000			50 000	
g12	60	6	80	4 800			6 000	
g13	108	12	1 350	145 800			150 000	

3.2.2 Evaluation results

The parameters set above are used for all 13 benchmark problems. The comparision experiments of CDPSO algorithm on each benchmark problem

are independently performed 30 runs, and the best, mean, the worst and standard deviations produced by CDPSO, SACABC, M-ABC, COMDE, and LCA algorithms are listed in Table 2.

Table 2 Optimization results of CDPSO algorithm compared to others

Function	Status	Method				
		SACABC[15]	M-ABC[16]	COMDE[17]	LCA[18]	CDPSO
g01	Best	−15.000	−15	−15.000	−15	−15.000
	Mean	−15.000	−15	−15.000	−15	−15.000
	Worst	−15.000	−15	−15.000	−15	−15.000
	St.d	0	0	1.97E−013	4.83E−011	9.11E−016
g02	Best	−0.803 618	−0.803 615	−0.803 619	−0.803 577	−0.803 619
	Mean	−0.788 6	−0.799 336	−0.801 238	−0.801 563	−0.802 723
	Worst	−0.768 8	−0.777 438	−0.785 265	−0.792 589	−0.794 662
	St.d	0.014 1	6.84E−003	5.00E−003	3.50E−003	2.80E−003
g03	Best	−1.000 5	−1.000	−1.000 000 049	−1.000 5	−1.000 5
	Mean	−1.000 4	−1.000	−1.000 000 027	−1.000 5	−1.000 5
	Worst	−0.999 7	−1.000	−0.999 999 94	−1.000 5	−1.000 5
	St.d	2.550 86E−004	4.68E−005	3.026E−008	5.51E−006	1.10E−015
g04	Best	−30 665.539	−30 665.539	−30 665.539	−30 665.538 7	−30 665.538 7
	Mean	−30 665.539	−30 665.539	−30 665.539	−30 665.538 7	−30 665.538 7
	Worst	−30 665.539	−30 665.539	−30 665.539	−30 665.538 7	−30 665.538 7
	St.d	0	2.22E−011	0	1.07E−011	1.05E−011
g05	Best	5 126.497	5 126.736	5 126.498 109 4	5 126.496 7	5 126.496 7
	Mean	5 126.497	5 178.139	5 126.498 109 4	5 126.496 7	5 126.496 7
	Worst	5 126.497	5 317.197	5 126.498 109 4	5 126.496 7	5 126.496 7
	St.d	9.586 9E−013	5.61E+001	0	9.70E−013	9.56E−013
g06	Best	−6 961.814	−6 961.814	−6 961.813 875	−6 961.813 9	−6 961.813 876
	Mean	−6 961.814	−6 961.814	−6 961.813 875	−6 961.813 9	−6 961.813 876
	Worst	−6 961.814	−6 961.814	−6 961.813 875	−6 961.813 9	−6 961.813 876
	St.d	1.917 4E−012	0	0	1.85E−012	1.73E−012
g07	Best	24.306 2	24.315	24.306 209	24.306 209 08	24.306 209 07
	Mean	24.306 2	24.415	24.306 209	24.306 222 27	24.306 209 07
	Worst	24.306 4	24.854	24.306 211	24.306 482 68	24.306 209 07
	St.d	2.543 4E−007	1.24E−01	4.70E−007	4.95E−012	3.29E−012
g08	Best	−0.095 825	−0.095 825	−0.095 825	−0.095 825 04	−0.095 825 04
	Mean	−0.095 825	−0.095 825	−0.095 825	−0.095 825 04	−0.095 825 04
	Worst	−0.095 825	−0.095 825	−0.095 825	−0.095 825 04	−0.095 825 04
	St.d	1.462 8E−017	4.23E−017	9.00E−018	2.82E−017	2.85E−017
g09	Best	680.630	680.632	680.630 057	680.630 057	680.630 057
	Mean	680.630	680.647	680.630 057	680.630 057	680.630 057
	Worst	680.630	680.691	680.630 057	680.630 057	680.630 057
	St.d	1.198 4E−013	1.55E−002	4.071E−013	9.81E−012	1.28E−013
g10	Best	7 049.248	7 051.706	7 049.248 020	7 049.248 020 6	7 049.248 020 0
	Mean	7 049.248	7 233.882	7 049.248 077	7 049.248 054 2	7 049.248 030 9
	Worst	7 049.248	7 473.109	7 049.248 615	7 049.248 281 6	7 049.248 173 1
	St.d	3.031 6E−013	1.10E+002	1.50E−004	5.80E−005	3.37E−005
g11	Best	0.749 9	0.75	0.749 999	0.749 9	0.749 9
	Mean	0.749 9	0.75	0.749 999	0.749 9	0.749 9
	Worst	0.749 9	0.75	0.749 999	0.749 9	0.749 9
	St.d	1.170 2E−016	2.30E−005	0	1.13E−016	1.12E−016
g12	Best	−1.000	−1.000	−1.000 000	−1	−1
	Mean	−1.000	−1.000	−1.000 000	−1	−1
	Worst	−1.000	−1.000	−1.000 000	−1	−1
	St.d	0	0	0	0	0
g13	Best	0.053 94	0.053 985	0.053 941 5	0.053 941 514	0.053 941 514
	Mean	0.092 42	0.158 552	0.053 941 5	0.053 941 514	0.053 941 514
	Worst	0.438 802	0.442 905	0.053 941 5	0.053 941 514	0.053 941 514
	St.d	0.121 7	1.73E−001	1.40E−017	3.97E−017	1.86E−017

The numerical results obtained by using CDPSO algorithm and other four algorithms are analyzed according to their robustness, search quality and computational cost. As shown in Table 2, CDPSO algorithm is better or no worse than the other four algorithms in terms of the "best" "mean" and "worst" objective functions for all 13 benchmark problems, which means that CDPSO algorithm is better than the other four algorithms in search quality. In terms of standard deviation, since CDPSO algorithm is designed to reduce the calculation cost and improve the calculation efficiency, FFEs are set very small, so it is not common in most problems, but the order of magnitude is already small enough. Moreover, its standard deviation will be much smaller if FFEs are properly improved, thus the robustness is not poor. In terms of computational cost, it is measured by FFEs. CDPSO algorithm has the lowest cost for 10 benchmark problems, which is 2.8%—52% lower than the lowest cost algorithm in literatures. In particular, in g03, the optimal solution and the minimum variance are obtained using only 48% of the computational cost of COMDE. Although in g02, g06 and g10, this method does not have a good advantage over FEEs, which may be caused by strong suboptimal solution in the problem. However, the proposed algorithm achieves the best optimization effect in these three problems after slightly enlarging the FEE, which further illustrates the advantage of CDPSO algorithm in search capability.

4 Experiment and Results

4.1 Experiment parameters

Before the experiment, machine parameters, tool parameters, workpiece parameters and other parameters related to optimization are shown in Tables 3—8. Besides, the machining process is down milling, the total milling depth $d_{\text{totoal}} = 20$ mm and the required surface roughness $R_{\max} = 6.4$ μm.

Table 3 Machine parameters

Maximum spindle speed / ($r \cdot min^{-1}$)	Spindle power / kW	Rated torque / (N•m)
24 000	8.2	4

Table 4 Tool parameters

Material	Diameter / mm	Number of teeth	Nose radius / mm	Tool life / min
Cemented carbide	10.0	3	0.2	240

Table 5 Workpiece parameters

Material	Size / (mm×mm×mm)	Cutting force parameter	
		Tangential cutting force coefficient / ($N \cdot mm^{-2}$)	Normal cutting force coefficient / ($N \cdot mm^{-2}$)
AL2A12	100×50×40	863.4	225.3

Table 6 Modal parameters of machine tool-tool system

Natural frequency / Hz	Damping ratio	Modal mass / kg
1 235.85	0.029 9	0.111 3

Table 7 Value range of machining parameters

Process stage	Spindle speed / ($r \cdot min^{-1}$)	Feed per tooth / ($mm \cdot (tooth)^{-1}$)	Axial cutting depth / mm	Radial cutting depth / mm
Rough	5 000—20 000	0.03—0.10	1.0—3.0	0.50—10.0
Semi-finish	5 000—20 000	0.03—0.10	1.0—3.0	0.50—10.0
Finish	5 000—20 000	0.01—0.03	0.1—0.2	0.50—10.0

Table 8 Other parameters related to the optimization model

C_u	K_u	p_u	q_u	s_u	x_u	y_u	C_v	K_v
534.6	1	1	1	1	0.9	0.74	445	1
q_v	x_v	y_v	s_v	p_v	l			
0.2	0.15	0.35	0.2	0	1.00			

The 3-D SLD based on the above parameters is obtained as Fig.3. The accuracy of the machining stability prediction model based on 2ndFDM has been described[4], and the 3-D machining stability model in this study is a 3-D extension based on the original model. Therefore, there is no need to con-

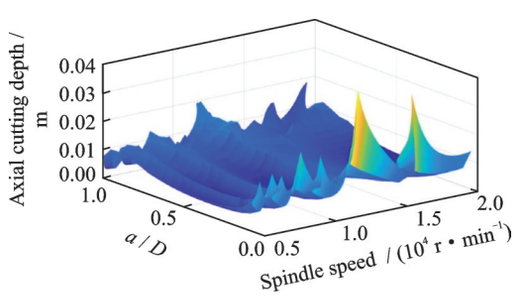

Fig.3 2ndFDM-based 3-D SLD

duct redundant demonstration for its accuracy.

4.2 Experimental results

The milling experiments are conducted based on the empirical parameters and the parameters obtained through the optimization model of machining parameters proposed in this study. The corresponding production time is shown in Table 9.

According to the optimization results, the optimal parameters are obtained at 100% radial cutting depth (slotting), and the corresponding stable boundary is shown in Fig.4. In the figure, the three points are machining parameters corresponding to rough machining, semi-finishing and finishing, respectively, which can verify that the three sets of parameters meet the stability constraint of milling.

Table 9 Comparison of parameter optimization results of multi-pass milling

Types of machining parameter	Process stage	Number of passes	Axial cutting depth/mm	Radial cutting depth/mm	Spindle speed / (r•min^{-1})	Feed per tooth / (mm•(tooth)$^{-1}$)	Processing time / min
Empirical parameter	Rough	7	2.5	5	6 000	0.05	8.333 2
	Semi-finish	1	2.4	5	6 000	0.03	
	Finish	1	0.1	5	8 000	0.03	
Optimal parameter	Rough	6	3.0	10	13 630.81	0.10	5.499 5
	Semi-finish	1	1.9	10	15 074.03	0.10	
	Finish	1	0.1	10	20 000.00	0.03	

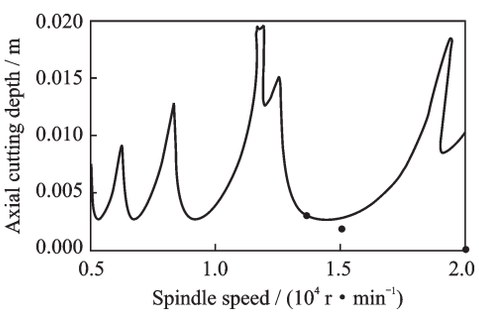

Fig.4 2ndFDM-based 2-D SLD

As shown in Table 9, the empirical process parameters are too conservative, which cannot effectively give play to the performance of the machine tool, and result in longer milling time. However, on the premise of guaranteeing the machining stability and workpiece surface quality, the optimal parameters effectively generate the performance of the machine tool, which greatly reduce the production time, effectively improve the processing efficiency, and further verify the practicability and effectiveness of the proposed optimization model and algorithm.

5 Conclusions

Optimization of machining parameters is of great importance for multi-pass end milling operations to shorthen production time and improve efficiency. However, there are few studies to introduce chatter stability constraint into optimization model. Moreover, nearly all of chatter stability models construct the stable domain about spindle speed and axial cutting depth only, without consideration of radial cutting depth. To solve the aforementioned problems, the main contributions of this study are as follows.

(1) A 2ndFDM-based 3-D stability prediction model is developed for simultaneously optimization of spindle speed, axial cutting depth and radial cutting depth.

(2) A parameter optimization model of multi-pass end milling is developed by taking number of passes, spindle speed, axial cutting depth, radial cutting depth and feed rate as design parameters to achieve the minimum production time while considering a large number of constraints including 3-D stability.

(3) An algorithm named CDPSO is proposed to solve the developed parameter optimization model and the evaluation results indicate that it has a certain advantage in the computational cost as well as comparable search quality and robustness.

(4) A demonstrative example indicates that the developed parameter optimization model and algo-

rithm are indeed practical.

References

[1] JAMIL M, HAQ E, KHAN A M, GUPTA M K, et al. Machinability investigation and optimization of process parameters in cryogenic assisted sustainable turning of AISI L6 tool steel[J]. Transactions of Nanjing University of Aeronautics and Astronautics, 2020, 37(3): 403-415.

[2] CHEN F F, XIANG J, THOMAS D G, et al. Model-based parameter optimization for arc welding process simulation[J]. Applied Mathematical Modelling, 2020, 81: 386-400.

[3] GHOSH G, MANDAL P, MONDAL S C. Modeling and optimization of surface roughness in keyway milling using ANN, genetic algorithm, and particle swarm optimization[J]. The International Journal of Advanced Manufacturing Technology, 2019, 100(5): 1223-1242.

[4] DING Y, ZHU L M, ZHANG X J, et al. Second-order full-discretization method for milling stability prediction[J]. International Journal of Machine Tools and Manufacture, 2010, 50(10): 926-932.

[5] QIN C, TAO J, SHI H, et al. A novel Chebyshev-wavelet-based approach for accurate and fast prediction of milling stability[J]. Precision Engineering, 2020, 62: 244-255.

[6] BUDAK E, TEKELI A. Maximizing chatter free material removal rate in milling through optimal selection of axial and radial depth of cut pairs[J]. CIRP Annals, 2005, 54(1): 353-356.

[7] CHEN D, LIN B, HAN Z, et al. Study on the optimization of cutting parameters in turning thin-walled circular cylindrical shell based upon cutting stability[J]. The International Journal of Advanced Manufacturing Technology, 2013, 69(1/2/3/4): 891-899.

[8] YANG J F, GE H J, YANG F. High-reliability photovoltaic converter based on improved PSO algorithm[J]. Transactions of Nanjing University of Aeronautics and Astronautics, 2018, 35(S1): 68-74.

[9] DEVARAJAIAH D, MUTHUMARI C. Fuzzy logic-integrated PSO methodology for parameters optimization in end milling of Al/SiCp MMC[J]. Journal of the Brazilian Society of Mechanical Sciences and Engineering, 2019. DOI: 10.1007/s40430-019-1725-8.

[10] LI D, LIU C, GAN W. A new cognitive model: Cloud model[J]. International Journal of Intelligent Systems, 2009, 24(3): 357-375.

[11] YANG W, GUO Y, LIAO W. Optimization of multi-pass face milling using a fuzzy particle swarm optimization algorithm[J]. The International Journal of Advanced Manufacturing Technology, 2011, 54(1/2/3/4): 45-57.

[12] HIGUCHI T, TSUTSUI S, YAMAMURA M. Theoretical analysis of simplex crossover for real-coded genetic algorithms[C]//Proceedings of International Conference on Parallel Problem Solving from Nature. Berlin, Heidelberg: Springer, 2000: 365-374.

[13] RUNARSSON T P, YAO X. Stochastic ranking for constrained evolutionary optimization[J]. IEEE Transactions on Evolutionary Computation, 2000, 4(3): 284-294.

[14] WANG Y, CAI Z, GUO G, et al. Multiobjective optimization and hybrid evolutionary algorithm to solve constrained optimization problems[J]. IEEE Transactions on Systems, Man, and Cybernetics, Part B (Cybernetics), 2007, 37(3): 560-575.

[15] LI X, YIN M. Self-adaptive constrained artificial bee colony for constrained numerical optimization[J]. Neural Computing and Applications, 2014, 24(3/4): 723-734.

[16] MEZURA-MONTES E, CETINA-DOMÍNGUEZ O. Empirical analysis of a modified artificial bee colony for constrained numerical optimization[J]. Applied Mathematics and Computation, 2012, 218(22): 10943-10973.

[17] MOHAMED A W, SABRY H Z. Constrained optimization based on modified differential evolution algorithm[J]. Information Sciences, 2012, 194: 171-208.

[18] KASHAN A H. An efficient algorithm for constrained global optimization and application to mechanical engineering design: League championship algorithm (LCA)[J]. Computer-Aided Design, 2011, 43(12): 1769-1792.

Acknowledgements This work is supported partially by the National Science Foundation of China (No.51775279), National Defense Basic Scientific Research Program of China (No.JCKY201605B006), Fundamental Research Funds for the Central Universities (No.NT2021019), Jiangsu Industry Foresight and Common Key Technology (No. BE2018127).

Authors Mr . **CAI Xulin** received the B.S. degree in mechanical design manufacturing and automation from Nanjing Agricultural University, Nanjing, China, in 2018. From 2018 to present, he is studying for the master degree of aerospace manufacturing engineering in College of Mechanical and Electrical Engineering, Nanjing University of Aeronau-

tics and Astronautics (NUAA), Nanjing, China. His research has focused on NC machining technology.

Dr. **YANG Wenan** received the Ph.D. degree in electronic engineering from NUAA in 2013. His current research interest is manufacturing informatics and quality engineering.

Author contributions Mr. **CAI Xulin** designed the dynamic prediction model, parameter optimization model and parameter optimization algorithm, and wrote the original manuscript. Dr. **YANG Wenan** designed and implemented the verification experiment, and participated in the manuscript writing and modification. Mr. **HUANG Chao** contributed to the discussion and background of the study. All authors commented on the manuscript and approved the submission.

Competing interests The authors declare no competing interests.

(Production Editor: XU Chengting)

基于云滴粒子群优化算法的多道次端铣削高效稳定切削参数优化方法

蔡旭林，杨文安，黄　超

(南京航空航天大学直升机传动技术国家重点实验室，南京 210016，中国)

摘要：多道次端铣削切削参数对加工时间和加工质量有着正面或负面的影响，因此对多道次端铣削加工参数的优化是非常重要的。本文建立了基于二阶全离散法(Second-order full-discrete method，2ndFDM)的三维稳定性预测模型，以同时优化主轴转速、轴向切深和径向切深。在综合考虑三维稳定性、机床性能、刀具寿命和加工要求的条件下，得到各道次的最佳加工参数，以达到最短的生产时间。同时提出了一种基于云滴的粒子群优化(Cloud drop-enabled particle swarm optimization，CDPSO)算法，并利用13个标准测试问题对CDPSO算法的性能进行了评估。数值结果表明，该算法在计算成本、搜索能力和鲁棒性方面具有一定优势。最后通过一个切削参数优化实例验证了所提方法在提升加工效率与稳定性方面的有效性。

关键词：切削参数；多道次端铣削；颤振稳定性；粒子群优化；云模型